Am. J. Hum. Genet. 67:549–562, 2000

Iron-Dependent Self-Assembly of Recombinant Yeast Frataxin: Implications for Friedreich Ataxia

Jiri Adamec,[1,2] Frank Rusnak,[2] Whyte G. Owen,[2] Stephen Naylor,[2] Linda M. Benson,[2] A. Marquis Gacy,[3] and Grazia Isaya[1,2]

Departments of [1]Pediatric & Adolescent Medicine, [2]Biochemistry & Molecular Biology, and [3]Pharmacology, Mayo Clinic and Foundation, Rochester, MN

Frataxin deficiency is the primary cause of Friedreich ataxia (FRDA), an autosomal recessive cardiodegenerative and neurodegenerative disease. Frataxin is a nuclear-encoded mitochondrial protein that is widely conserved among eukaryotes. Genetic inactivation of the yeast frataxin homologue (Yfh1p) results in mitochondrial iron accumulation and hypersensitivity to oxidative stress. Increased iron deposition and evidence of oxidative damage have also been observed in cardiac tissue and cultured fibroblasts from patients with FRDA. These findings indicate that frataxin is essential for mitochondrial iron homeostasis and protection from iron-induced formation of free radicals. The functional mechanism of frataxin, however, is still unknown. We have expressed the mature form of Yfh1p (mYfh1p) in *Escherichia coli* and have analyzed its function in vitro. Isolated mYfh1p is a soluble monomer (13,783 Da) that contains no iron and shows no significant tendency to self-associate. Aerobic addition of ferrous iron to mYfh1p results in assembly of regular spherical multimers with a molecular mass of ~1.1 MDa (megadaltons) and a diameter of 13 ± 2 nm. Each multimer consists of ~60 subunits and can sequester >3,000 atoms of iron. Titration of mYfh1p with increasing iron concentrations supports a stepwise mechanism of multimer assembly. Sequential addition of an iron chelator and a reducing agent results in quantitative iron release with concomitant disassembly of the multimer, indicating that mYfh1p sequesters iron in an available form. In yeast mitochondria, native mYfh1p exists as monomer and a higher-order species with a molecular weight >600,000. After addition of ^{55}Fe to the medium, immunoprecipitates of this species contain >16 atoms of ^{55}Fe per molecule of mYfh1p. We propose that iron-dependent self-assembly of recombinant mYfh1p reflects a physiological role for frataxin in mitochondrial iron sequestration and bioavailability.

Introduction

Iron is essential for many cellular functions, but free iron is extremely insoluble and is highly toxic at physiological pH under aerobic conditions (de Silva et al. 1996). To overcome these obstacles, bacterial and eukaryotic cells have adopted various mechanisms for the acquisition and intracellular storage of iron (de Silva et al. 1996; Harrison and Arosio 1996). There are no known mechanisms for iron management inside mitochondria, in spite of the fact that iron is required for heme and iron-sulfur cluster biosynthesis, and uncomplexed iron can react with hydrogen peroxide, a by-product of respiration, and generate highly toxic hydroxyl radicals (Wallace and Melov 1998). Although most iron is probably incorporated into heme and iron-sulfur clusters immediately after crossing the inner mitochondrial membrane, it seems logical that mitochondria should have some mechanism to chaperone and/or sequester uncomplexed iron and to release it when needed. The mitochondrial protein frataxin (Campuzano et al. 1997; Koutnikova et al. 1997) is a potential candidate to fulfill this function. The results of recent studies have shown that yeast frataxin (Yfh1p) is required for mitochondrial iron efflux (Radisky et al. 1999) and that lack of Yfh1p results in mitochondrial iron overload, which in turn leads to increased sensitivity to oxidant stress and loss of mitochondrial function (Babcock et al. 1997; Foury and Cazzalini 1997). A deficiency of human frataxin is responsible for Friedreich ataxia (FRDA [MIM 229300]), an autosomal recessive cardiodegenerative and neurodegenerative disease (Campuzano et al. 1996). Iron deposits, multiple iron-sulfur enzyme deficiencies, and reduced levels of mtDNA have been observed in cardiac tissue from patients with FRDA (Lamarche et al. 1980; Rotig et al. 1997; Bradley et al. 2000). In addition, hypersensitivity to oxidative stress that responds to iron chelators has been observed in cultured FRDA fibroblasts (Wong et

Received June 16, 2000; accepted for publication July 18, 2000; electronically published August 4, 2000.

Address for correspondence and reprints: Dr. Grazia Isaya, Mayo Clinic, 200 First Street SW, Hilton 210, Rochester, MN 55905. E-mail: isaya@mayo.edu

0002-9297/2000/6703-0003$02.00

al. 1999). These findings indicate that frataxin is essential for mitochondrial iron homeostasis and for relief from free radical toxicity in yeast and humans as well. The functional mechanism of frataxin, however, is unknown. A direct role in iron export across the inner mitochondrial membrane seems unlikely, in view of the hydrophilicity of frataxin (Knight et al. 1998; Branda et al. 1999) and the apparent lack of physical interaction between frataxin and other mitochondrial proteins involved in iron movement (Koutnikova et al. 1998). We have hypothesized that frataxin could instead serve as a means to sequester mitochondrial iron and maintain it in a bioavailable form. To begin to test this hypothesis, we have analyzed the ability of a recombinant yeast frataxin polypeptide (mYfh1p) to sequester and release iron in vitro. We describe the iron-dependent self-assembly of mYfh1p and discuss its possible implications for frataxin function in vivo.

Material and Methods

Plasmids and Strains

The primers used for the Yfh1p(V60M) construct were a forward primer including an *Eco*RI site, a Kozak sequence (Kozak 1987), and the 5′ end of the *YFH1* (GenBank accession number Z74168) coding sequence (5′-agaattcgccgccaccatgattaagcggtctctcgcaag-3′), and a reverse primer including codons 54–65 of *YFH1,* with a GTT→ATG change at codon 60 (5′-acttcttgaggcaccatttgaccatctgtcgagg-3′). The PCR product was coupled with a reverse primer including the 3′ end of the *YFH1* coding sequence, a stop codon, and a *Sal*I site (5′-atatatgtcgaccttattggcttttagaaatggccttc-3′). The final PCR product was cloned into pGEM-4 (Promega) and was sequenced completely, yielding pGEM-YFH1(V60M). The primers used to generate a PCR product for the mYfh1p expression construct were a forward primer including an *Nde*I site, an ATG codon, and codons 53–62 of *YFH1* (5′-tattattacatatggaatcctcgacagatggtcaagttgtgcc-3′), and a reverse primer including the 3′ end of the *YFH1* coding sequence, a stop codon, and a *Bam*HI site (5′-tatataggatccattattggcttttagaaatggccttctcaac-3′). This product was cloned into pET24a(+) (Novagen) downstream of the T7 promoter and was sequenced completely, yielding pETYF-1, which was transformed into *Escherichia coli* strain BL21(DE3) (Novagen) to produce the BL21 (DE3)[pETYF-1] strain.

Expression and Purification of Recombinant mYfh1p

An overnight culture of BL21(DE3)[pETYF-1] was inoculated into 500 ml Luria broth containing 30 μg kanamycin per ml. Cells were grown to an OD_{600} of ~0.7, and mYfh1p expression was induced with 0.5 mM isopropyl-β-D-thiogalactopyranoside for 2 h at 37°C. Cells (wet weight 4 g) were harvested, washed, and resuspended in 10 ml of 20 mM Tris-HCl, pH 8.0, 50 mM NaCl (TN50) and were disrupted by sonication. After centrifugation at 25,000 × *g* for 20 min at 4°C, the supernatant (total protein 195 mg) was loaded on an MT20 column packed with Macro-Prep DEAE (Bio-Rad). The column was washed with 140 ml TN50, and mYfh1p was eluted by a 400-ml linear gradient from 50–550 mM NaCl in 20 mM Tris-HCl, pH 8.0. Fractions containing mYfh1p were pooled and concentrated to 1 ml, were diluted to 4 ml with TN50, and were loaded on a UNO Q1 column (Bio-Rad). The column was washed with 26 ml TN50, and mYfh1p was eluted by a 40-ml linear NaCl gradient, as described above. Fractions were pooled, concentrated to 1 ml, and loaded on a Superdex 200 column (Pharmacia). Recombinant mYfh1p was eluted with 10 mM HEPES-KOH, pH 7.4, 100 mM NaCl. Fractions were pooled, concentrated to 2.5 ml, and desalted into 10 mM HEPES-KOH, pH 7.4 (HEPES buffer), through a NAP-25 column (Pharmacia); protein aliquots (2 mg/ml) were stored at −70°C. All steps were performed at 4°C, with use of a BioLogic HR Workstation (Bio-Rad). Microelectrospray ionization mass spectrometry was performed on isolated mYfh1p (36 μM) in 10 mM ammonium bicarbonate, by means of direct infusion (3 μl/min) in a Finnigan-Mat 900 Mass Spectrometer, as described elsewhere (Veenstra et al. 1998). Iron concentration was determined by inductively coupled plasma emission spectroscopy (ICP) on an Optima ICP (PE Biosystems) (Nixon et al. 1986).

Gel Filtration

High-resolution columns (16 mm × 50 cm) were packed with 100 ml Superdex 200 preparative grade or Superose 6 (Pharmacia) and were equilibrated with HEPES buffer, 100 mM NaCl. Blue Dextran 2000 (1 mg/ml) was used to estimate void volumes, and molecular-weight (MW) standard mixtures were used for calibrations. Samples (1 ml) were loaded using a static loop (1 ml) and were eluted with HEPES buffer, 100 mM NaCl. Samples were prepared by incubating mYfh1p with $Fe(NH_4)_2(SO_4)_2$ or other metals (Sigma) at the required concentrations in 1 ml HEPES buffer for 1 h at 30°C. After centrifugation at 14,000 × *g* for 5 min, the supernatant was immediately applied to the column.

Iron Release

Isolated mYfh1p (120 μM) was incubated with $Fe(NH_4)_2(SO_4)_2$ at an Fe:mYfh1p ratio of 30:1, and the sample was passed through a NAP-25 column to remove unbound iron and was divided into two aliquots. The total iron content in the sample was determined by ICP.

Buffer and stock solutions and Fe-mYfh1p were made anaerobic by purging with oxygen-free (<0.5 ppm) argon with the use of septa-sealed vials, and they were added, by means of a gas-tight syringe, to an anaerobic 3-ml quartz cell in a Cary 1 spectrophotometer (Richards et al. 1996). First, the chelator α,α'-bipyridine (BIPY) was added anaerobically, and the absorbance (A) was zeroed at 520 nm, which is the wavelength maximum of $Fe(BIPY)_3^{2+}$ (Richards et al. 1996). The reaction was started by the anaerobic addition of Fe-mYfh1p (total protein 240 μg), and A_{520} versus time (A_{520}/time) was measured until the absorbance reached a constant value. An anaerobic solution of sodium dithionite in 100 mM HEPES buffer, pH 7.4, was added at 30 min (final concentration 1 mM), and measurements of A_{520}/time were continued until a new constant value was reached. The final concentrations of mYfh1p and BIPY were 6 μM and 1 mM, respectively, and the extinction coefficient of $Fe(BIPY)_3^{2+}$ at 520 nm is much higher than that of iron-loaded mYfh1p (9,000 vs. 200 $M^{-1}cm^{-1}$ per mol of iron). Therefore, the absorbances measured in this experiment reflect formation of $Fe(BIPY)_3^{2+}$, providing an accurate measurement of the amount of iron released from Fe-mYfh1p.

Sedimentation Equilibrium Analysis

Isolated mYfh1p (8 μM) was incubated with 320 μM $Fe(NH_4)_2(SO_4)_2$ as described in the Gel Filtration section. The sample was centrifuged and was passed through a NAP-25 column, and it was diluted, with HEPES buffer, to A_{280} = ~0.3. Samples in aluminum-filled epon (double-sector) centerpieces were layered over perfluorohexane to a fluid height of 5–6 mm (0.2 ml). After 2 h at 18,000 rpm, the samples were centrifuged to equilibrium for 16 h at 6,000 rpm at 17°C in a Beckman Prep-Scanner analytical ultracentrifuge (Williams et al. 1958). Cells were scanned with a 200-μm slit and a bandpass filter of 280 ± 10 nm.

Electron Microscopy and Atomic Force Microscopy

Isolated mYfh1p (40 μM) was incubated with 1.6 mM $Fe(NH_4)_2(SO_4)_2$ to a final Fe:mYfh1p ratio of 40:1, and it was chromatographed through the Superdex 200 column as described in the Gel Filtration section. Fractions corresponding to the 1.1-MDa form (fractions 3–5; see fig. 2*D*) in 10 mM HEPES-KOH, pH 7.4, 100 mM NaCl, were diluted with distilled water and were reconcentrated, by use of an Ultrafree-4 cell (Millipore), to a final mYfh1p concentration of 20 μM and a final iron concentration of 1 mM in 0.02 mM HEPES-KOH, pH 7.4, 0.2 mM NaCl. An aliquot was visualized by negative staining with 0.5% uranyl acetate in a JEOL 1200 EX II microscope at 60 kV (primary magnification × 50,000). Another aliquot was placed on a grid and was dried. With no additional preparation, this sample was analyzed by electron microscopy (EM) and then by atomic force microscopy (AFM) (Hansma and Hoh 1994). AFM imaging was performed using tapping mode in air with 125-μm silicon TESP tips in a NanoScope III MultiMode system (Digital Instruments). The tapping frequency was 288.2 kHz, and the scanning frequency was 1 Hz. AFM images were analyzed using Digital Instruments NanoScope IIIa software. Three-dimensional images were generated from topographic height information and were illuminated from various angles.

In Vivo Studies

Yeast cells were grown in rich medium containing 2% galactose to late log phase, and mitochondria were isolated (Branda et al. 1999), were diluted to a protein concentration of 5 mg/ml in 10 mM HEPES buffer containing 1 tablet/100 ml of complete EDTA-free protease inhibitors (Boehringer Mannheim) and 0.375 % Triton X-100, and were incubated for 30 min on ice with occasional agitation. This was followed by centrifugation at 165,000 × *g* for 30 min at 4°C to remove insoluble material. The supernatant (total protein ~3 mg) was concentrated to 1 ml by use of an Ultrafree-4 cell and was directly applied to a Superdex 200 column. Ten fractions (5 ml each) were collected, and 1.5-ml aliquots were concentrated and were analyzed by western blotting using anti-Yfh1p antibody (Branda et al. 1999). In immunoprecipitation experiments, yeast cells were grown as described above, except that the medium was supplemented with $^{55}FeCl_3$ to a final iron concentration of 0.4 μM. Mitochondria were isolated and detergent-extracted, and the supernatants (total cpm ~1.5–2.7 × 10^6) were fractionated on the Superdex 200 column as described above. The fractions were pretreated with 100 μl protein A-Sepharose (beads). After removal of the beads, the supernatants were incubated with anti-Yfh1p antibodies, and the immunocomplexes were precipitated with an additional 100 μl protein A-Sepharose (I.P.). The I.P. pellets were washed with 10 mM HEPES-KOH, pH 7.4, and 100 mM NaCl, after which the beads and the I.P. pellets were resuspended in the same buffer and were counted.

Results

Recombinant mYfh1p Is Isolated from Bacterial Cells as a Soluble Iron-Free Monomer

Similar to most mitochondrial proteins, Yfh1p is initially translated in the cytoplasm as a larger precursor protein (Knight et al. 1998). The precursor is imported into mitochondria and is processed to the mature form (mYfh1p), in two sequential steps, by the mitochondrial-processing peptidase (MPP) (Branda et al. 1999). We

determined the N-terminus of mYfh1p by means of in vitro processing with purified MPP and radiosequencing (fig. 1*A*), expressed a recombinant mYfh1p protein in *E. coli*, and purified it to homogeneity in three steps (fig. 1*B*). The purified protein migrated on SDS/PAGE with an apparent MW of ~20,000 (fig. 1*B*), an MW that was higher than the predicted MW of ~14,000. This abnormal mobility was previously reported by Knight et al. (1998) and Branda et al. (1999) and is explained by the acidic nature of the protein (calculated isoelectric point 4.34). Similarly, purified mYfh1p was eluted from a Superdex 200 column with an apparent MW of ~18,000 (fig. 2*A*). Microelectrospray ionization mass spectrometry of the purified protein, however, revealed a predominant (>95%) ion species with an MW of 13,783, an MW that precisely corresponds to the calculated MW of recombinant mYfh1p. ICP spectroscopy of the purified protein detected only background levels of iron. Isolated mYfh1p is therefore a soluble monomer that contains essentially no iron.

Iron Induces a High-MW Soluble Form of mYfh1p

To test whether iron can influence the behavior of mYfh1p, we incubated 320 μM $Fe(NH_4)_2(SO_4)_2$ at neutral pH under aerobic conditions in the absence or presence of isolated mYfh1p (8 μM; Fe:mYfh1p ratio 40:1). Both samples turned yellow, indicating oxidation of Fe^{2+} to Fe^{3+}. A large ferric oxyhydroxide precipitate formed in the first sample, but there was no detectable protein or iron precipitation in the sample containing mYfh1p (fig. 1*C*). We subsequently incubated mYfh1p (8 μM) with either $Fe(NH_4)_2(SO_4)_2$ (320 μM) or different divalent cations (320 μM), and we analyzed these samples by means of gel filtration on a Superdex 200 column (fractionation range 10–600 kDa). Whereas monomer was detected in the absence of added metals (fig. 2*A*, *peak 1*), incubation of mYfh1p with $Fe(NH_4)_2(SO_4)_2$ yielded a high-MW species (fig. 2*C*, *peak 2*) that exceeded the size range of the column. Peak 2 exhibited a 6-fold increase in A_{280} relative to peak 1; the absorbance of ferric oxides (ϵ_{280} = 160,000 $M^{-1}cm^{-1}$) in peak 2

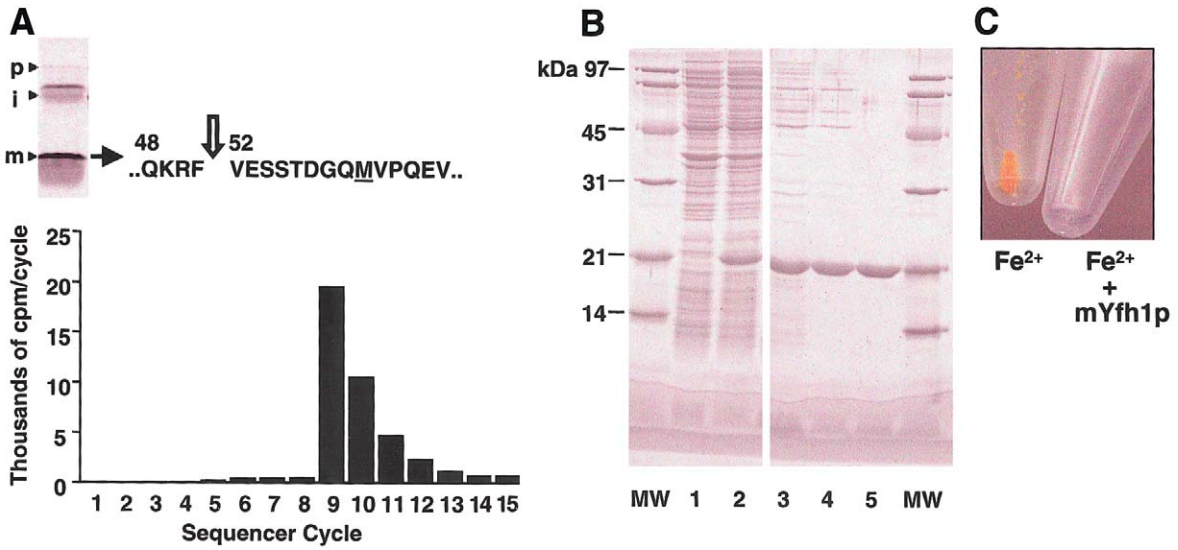

Figure 1 Production of recombinant mYfh1p. *A,* N-terminal radiosequencing of mYfh1p. *Top,* Two-step processing of Yfh1p by purified MPP, with "p," "i," and "m" denoting the precursor, intermediate, and mature forms of Yfh1p, as analyzed by 12% SDS/PAGE (Branda et al. 1999). A methionine residue (*underlined*) was substituted for valine 60 downstream of the predicted second MPP cleavage site to provide a radioactive marker, and [^{35}S]methionine-pYfh1p(V60M) precursor was incubated with recombinant yeast MPP (Branda et al. 1999). Processing products were separated by SDS/PAGE, were electroblotted onto a polyvinylidene difluoride membrane, and were detected by autoradiography. The mYfh1p band was excised and applied directly on a PE/ABD Procise 494-HS sequencer, and 100% of each fraction was collected and was analyzed by scintillation counting (Matsudaira 1987). Valine 52 marks the N-terminus of mYfh1p, as determined by the release of [^{35}S]methionine in cycle 9; note that, in the following cycles, the cpm decreased by ~50% until reaching the level of background measured before cycle 9, as a result of insufficient washing of the cartridge and the line to the fraction collector. The identified cleavage site, RF↓VE, matches the consensus, Rx↓(S/x), found at many MPP cleavage sites (Gavel and von Heijne 1990). *B,* Overexpression and purification of mYfh1p. Aliquots of different fractions were analyzed by 12% SDS/PAGE and SYPRO Orange (Molecular Probes) staining. MW = MW marker proteins (1 μg protein/band). *Lanes 1–2* show bacterial lysate (20 μg) before and after induction, respectively; *lane 3,* Macro-Prep DEAE pool (9 μg); *lane 4,* UNO Q1 pool (4.5 μg); and *lane 5,* Superdex 200 pool (4 μg). *C,* Isolated mYfh1p maintains iron in a soluble form. A 320-μM solution of $Fe(NH_4)_2(SO_4)_2$ in 10 mM HEPES-KOH, pH 7.4, was incubated for 1 h at 30°C in the absence or presence of 8 μM mYfh1p. Both samples were centrifuged at 14,000 × *g* for 5 min, and the supernatants were removed before photography.

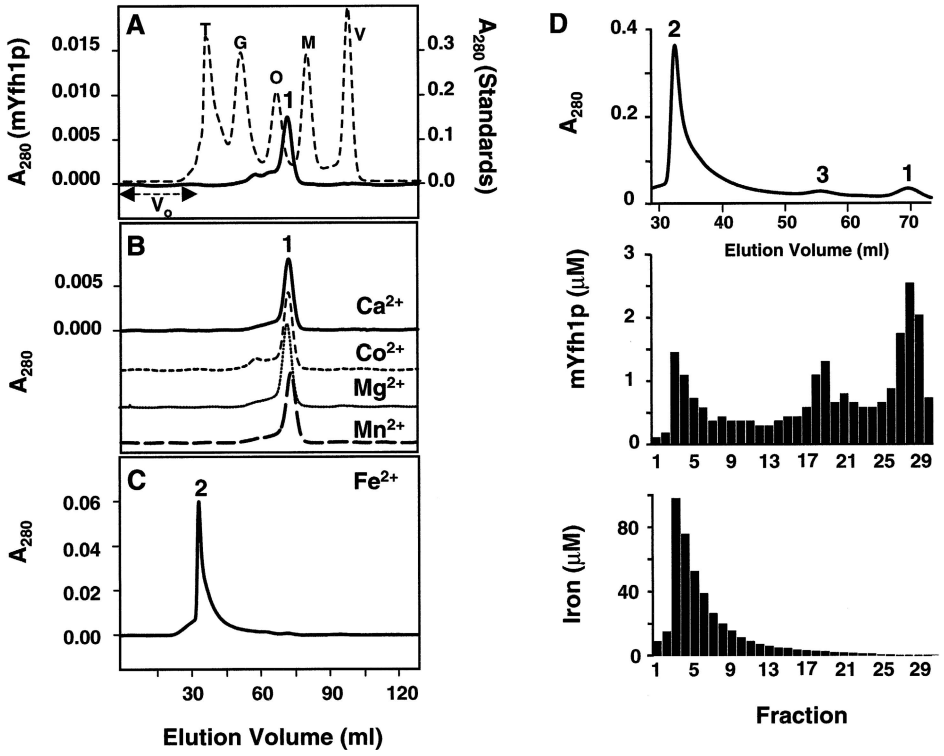

Figure 2 Iron induces self-assembly of mYfh1p. *A,* Purified mYfh1p (total protein 110 μg; final concentration 8 μM) was incubated in a final volume of 1 ml HEPES buffer for 1 h at 30°C, and the sample was centrifuged at 14,000 × *g* for 5 min and was immediately applied to a Superdex 200 column. V_0 = void volume. The elution profile of isolated mYfh1p is superimposed on that of MW standards (*broken line*). V = vitamin B_{12} (1.4 kDa); M = myoglobin (17 kDa); O = ovalbumin (44 kDa); G = gammaglobulin (158 kDa); T = thyroglobulin (669 kDa). *B,* Conditions were the same as those described for panel *A*, except that mYfh1p was incubated in the presence of 320 μM $CaCl_2$, $CoCl_2$, $MgCl_2$, or $MnCl_2$. The four chromatograms are superimposed. The A_{280} scale is shown only for the top chromatogram. *C,* Conditions were the same as those described for panel *A*, except that the incubation step was performed in the presence of 320 μM $Fe(NH_4)_2(SO_4)_2$. Note that most of the A_{280} of peak 2 is accounted for by the absorbance of ferric oxides (ϵ_{280} = 160,000 M^{-1} cm^{-1}), rather than the absorbance of mYfh1p (ϵ_{280} = 20,000 M^{-1} cm^{-1}). *D,* Conditions were the same as those described for panel *C,* except that 440 μg total protein (final concentration 8 μM) were used; the relevant portion of the chromatogram is shown (*top*). *Middle,* Protein concentration in the eluted fractions was analyzed by 12% SDS/PAGE, followed by staining with SYPRO Orange and densitometry in a Storm 840 Optical Scanner using the ImageQuant software package (Molecular Dynamics); a known amount (as determined by quantitative amino acid analysis) of purified mYfh1p was used as the internal standard. *Bottom,* Iron concentration was determined in the eluted fractions by ICP.

accounts for this increase. One possible explanation for this result is that, at neutral pH, the acidic nature of mYfh1p makes it prone to interact with ferric oxides, leading to formation of nonspecific aggregates. However, fractions corresponding to peak 2 could be stored at different temperatures (23°C or 4°C) for several days, or they could be concentrated to at least 1.5 mg protein per ml without any obvious protein or iron precipitation, demonstrating a degree of solubility uncharacteristic of nonspecific aggregates. Thus, an alternative explanation is that peak 2 reflects a controlled assembly process. This process was specifically induced by iron, because mYfh1p did not show any tendency to self-associate upon incubation with 320 μM $CaCl_2$, $CoCl_2$, $MgCl_2$, or $MnCl_2$ (fig. 2*B*). In addition, peak 2 did not form in the presence of 6 M urea or anti-Yfh1p antibodies (data not shown).

Stepwise Assembly of mYfh1p

To distinguish between aggregation and a specific assembly process, a larger amount of mYfh1p was incubated with $Fe(NH_4)_2(SO_4)_2$ (Fe:mYfh1p ratio 40:1), and the sample was analyzed on the Superdex 200 column (fig. 2*D*). Under these conditions, we detected peak 2, but we also detected monomer (peak 1) and an intermediate peak corresponding to an MW of ~93,000 (peak 3) (fig. 2*D, top*). The results of SDS/PAGE and ICP analysis showed that most input mYfh1p (>95%) was recovered in fractions 1–30, along with 50% (35 μg) of the input iron. Of the input mYfh1p, ~70% was assembled into higher-MW species (fractions 1–26), with peak 2 and peak 3 representing the predominant forms (fig. 2*D, middle*), whereas ~30% of the input mYfh1p was eluted as monomer (fractions 27–29). Contrary to

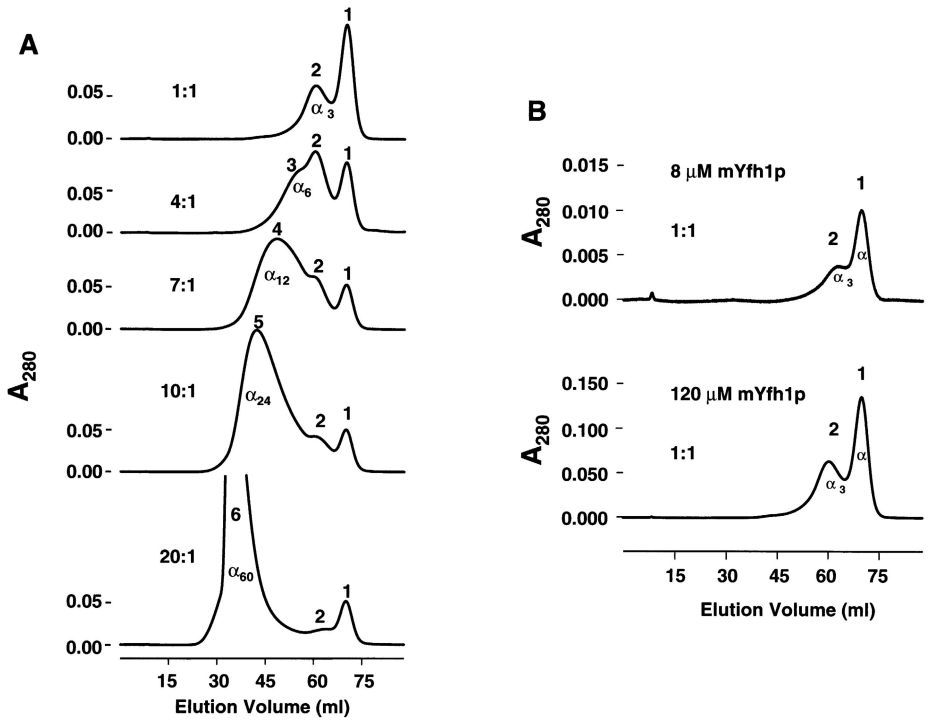

Figure 3 Iron-dependent stepwise assembly of mYfh1p. *A*, Fixed amount of mYfh1p (final concentration 120 μM [15-fold higher than that which was used in fig. 2*C–D*]) was incubated with increasing concentrations of $Fe(NH_4)_2(SO_4)_2$ to obtain the Fe:mYfh1p ratios indicated. Each sample was separately analyzed on the Superdex 200 column. *B*, As described for panel *A*, except that two different concentrations of mYfh1p were used.

what might be expected from a nonspecific aggregation process, the iron distribution among these three species was not a function of the protein concentration. Peak 1 (fractions 27–29) showed a protein concentration of 1.7–2.5 μM and ⩽0.4 atoms of iron per molecule of mYfh1p (fig. 2*D*, *bottom*). Peak 3 (fractions 18–20) and peak 2 (fractions 3–5) showed very similar protein concentrations (0.6–1.3 and 0.7–1.8 μM, corresponding to ~14% and 15% of the input protein, respectively) (fig. 2*D*, *middle*), but they showed a 30-fold difference in iron content (1.8–2.7 vs. 50–100 μM, corresponding to ~1% and 26% of the input iron, respectively) (fig. 2*D*, *bottom*). These data are consistent with a stepwise assembly process that increases the iron-binding capacity of mYfh1p without a concomitant increase in the absolute protein concentration. A specific assembly process is also supported by the inability of 30% of the input mYfh1p to form higher-order species. A fraction of iron-free monomer was consistently observed in independent assembly reactions and with different protein preparations, and this may reflect a protein fold that is not compatible with assembly.

Stepwise Assembly of mYfh1p Depends on the Molar Fe:mYfh1p Ratio

A fixed amount of mYfh1p (final concentration 120 μM) was treated with increasing concentrations of $Fe(NH_4)_2(SO_4)_2$ and was analyzed on the Superdex 200 column. Protein concentration was increased 15-fold, compared with that in the experiments shown in figure 2, to enable determination of the protein concentration in Superdex 200 fractions by means of amino acid analysis (fig. 3*A*). At an Fe:mYfh1p ratio of 1:1, we detected only the monomer (peak 1; MW ~18,000; α) and a second species (peak 2; MW ~50,000) that may correspond to the mYfh1p trimer (α_3). Increasingly larger species were detected at ratios of 4:1 (peak 3; MW ~93,000; α_6), 7:1 (peak 4; MW ~178,000; α_{12}), 10:1 (peak 5; MW ~331,000; α_{24}), and 20:1 (peak 6; MW >600,000; this species corresponds to peak 2 in fig. 2*D* and is denoted as α_{60} on the basis of the results of analyses described in the mYfh1p Assembles into Homogeneous Multimers of ~1.1 MDa section). The intensity of peak 1 decreased at Fe:mYfh1p ratios of 1:1–7:1, but it did not decrease any further at higher ratios (fig. 3*A*), a finding that is consistent with a fraction of monomer that is not competent for assembly, as noted in figure 2*D*. These data suggest that there is an initial step, in which an increasing fraction of monomer is assembled into $\alpha_3 \rightarrow \alpha_6 \rightarrow \alpha_{12}$, and a subsequent step, in which α_{12} is assembled into α_{60} without any further monomer contribution. We repeated this experiment three times and obtained virtually identical chromatograms, a result

Table 1

Protein and Iron Content of mYfh1p Oligomers

Species	Input Fe:mYfh1p	Final Content mYfh1p (μM)	Final Content Fe (μM)	Fe:mYfh1p
Peak:				
1	7:1	3.48[a]	.36–0.71	.1–.2
2	4:1	2.83–3.92	13.21–15.88	3.7–4.9
3	4:1	1.60–2.10	11.61–15.89	6.4–8.0
4	7:1	2.39–2.61	29.82–30.63	11.4–12.8
5	10:1	2.54–3.19	49.64–58.57	15.6–22.4
6	20:1	1.70–2.43[b]	87.50–101.78	41.9–51.5

Note.—Fractions corresponding to the maxima of peaks 1–6 (shown in fig. 3*A*) were analyzed for protein and iron concentrations, by means of amino acid analysis and ICP, and the final Fe:mYfh1p ratio was calculated for each sample. The ranges of values measured in three independent experiments are shown, except where indicated by footnotes *a* and *b*. Note that peak 1 was analyzed at the input ratio of 7:1 and contained only background levels of iron.

[a] $n = 1$.

[b] $n = 2$.

indicating that stepwise assembly of mYfh1p is reproducible. In figure 3*B*, two different concentrations of mYfh1p (8 and 120 μM) were analyzed at an Fe:mYf1p ratio of 1:1. Both samples showed only monomer (peak 1) and trimer (peak 2). Furthermore, assembly of α_{60} required a ratio >20:1 at 120 μM mYfh1p, a ratio that is only two times lower than the 40:1 ratio required at 8 μM mYfh1p (fig. 2*D*). These data indicate that mYfh1p assembly depends on the molar Fe:mYfh1p ratio and not the absolute protein or iron concentration. To determine the Fe:mYfh1p content of the species in figure 3*A*, fractions corresponding to the peak maxima were subjected to amino acid analysis and ICP. The data in table 1 show that each peak was characterized by a certain Fe:mYfh1p content, with little variability among experiments. As already noted for peak 2 and peak 3 (see fig. 2*D*), the species in figure 3*A* showed similar protein concentrations but increasingly higher iron concentrations, consistent with structural changes that expand the iron-loading capacity of mYfh1p. The largest species (peak 6; α_{60}) contained 42–51 iron atoms per molecule of mYfh1p, corresponding to >3,000 atoms of iron per multimer.

mYfh1p Stores Iron in an Available Form

To define what form of iron is sequestered by mYfh1p, we analyzed the electronic spectra of Superdex 200 fractions corresponding to α_{60}. These samples exhibited broad UV/visible spectra (220–570 nm) with intense absorptions characteristic of oxo-to-metal charge transfer bands ($\epsilon_{330-390}$ = 3,600–1,600 $M^{-1}cm^{-1}$ and $\epsilon_{455-515}$ = 550–220 $M^{-1}cm^{-1}$ per mol of iron), characteristic of oxo-bridged ferric iron (Sanders-Loehr 1989). In agreement with this finding, low-temperature (3.0–150 K) electron paramagnetic-resonance (EPR) spectra of the same samples were devoid of resonances that can be assigned to mononuclear high-spin Fe^{3+} species—that is, α_{60} is EPR-silent over this temperature range, despite the presence of highly paramagnetic ferric ions. These data are consistent with the presence of antiferromagnetically coupled ferric iron pairs, such as those are found in the iron core of ferritin (Chasteen et al. 1985). To analyze whether this iron can be released from mYfh1p, isolated protein (120 μM) was incubated with $Fe(NH_4)_2(SO_4)_2$ at an Fe:mYfh1p ratio of 30:1, which yields primarily α_{60} and monomer. In one-half of this sample, iron release was measured by successive addition of a specific Fe^{2+} chelator (BIPY) and the reducing agent dithionite under anaerobic conditions (Richards et al. 1996). We observed two consecutive iron-release reactions (fig. 4*A*) corresponding to the release of 40% and 60%, respectively, of the total iron in the sample. This result is consistent with the presence of a smaller group of readily released Fe^{2+} ions, which can be chelated by BIPY, and a larger group of Fe^{3+} ions, which can be chelated by

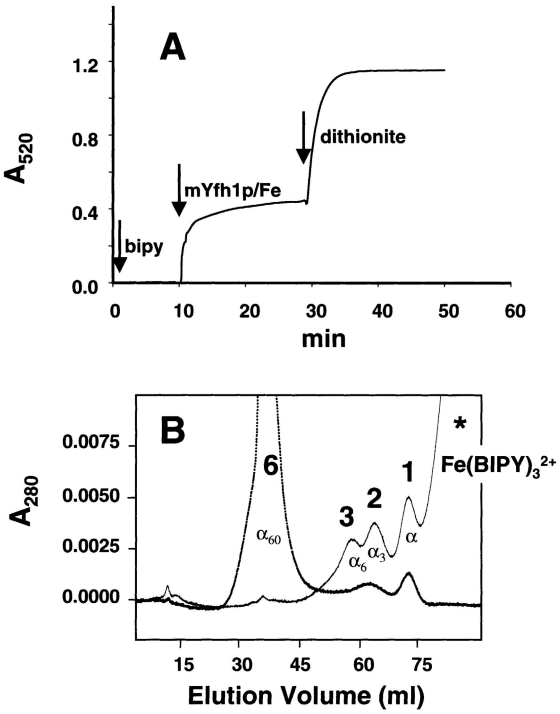

Figure 4 Iron release from mYfh1p. *A*, Chelator BIPY was loaded anaerobically into a Cary 1 spectrophotometer, and the absorbance was zeroed at 520 nm (*left arrow*). The reaction was started by anaerobic addition of Fe-mYfh1p (*middle arrow* [at 10 min]), and A_{520}/time was measured until the absorbance reached a constant value. An anaerobic solution of sodium dithionite was added at 30 min (*right arrow*), and measurements of A_{520}/time were continued until a new constant value was reached. *B*, Immediately afterward, the untreated and BIPY/dithionite-treated aliquots (80 μg total protein each) were separately analyzed on the Superdex 200 column.

BIPY only after reduction by dithionite. The two halves of the assembly mixture—before and after BIPY/dithionite treatment—were analyzed on the Superdex 200 column (fig. 4*B*). Peak 6 was the predominant species in the first aliquot, but it was no longer detected in the BIPY/dithionite-treated aliquot, which contained only monomer (peak 1; ~50%), trimer (peak 2; ~30%), and hexamer (peak 3; ~20%). On the basis of the Fe:mYfh1p content characteristic of peak 2 (~4 Fe/mYfh1p), peak 3 (~7 Fe/mYfh1p), and peak 6 (~50 Fe/mYfh1p) (table 1), we calculated that <5% of the iron was still bound to mYfh1p after BIPY/dithionite treatment, consistent with the degree of iron release determined in figure 4*A*. These data demonstrate that iron is stored in an available form in mYfh1p multimers and that self-assembly of mYfh1p is a reversible process.

mYfh1p Assembles into Homogeneous Multimers of ~1.1. MDa

To measure the MW of the iron-bound forms of mYfh1p, purified protein (8 μM) was incubated with $Fe(NH_4)_2(SO_4)_2$ (Fe:mYfh1p ratio 40:1), and the sample was applied to a Superose 6 column (fractionation range 5–5,000 kDa) (fig. 5*A*). The chromatogram showed a major peak with an apparent MW of ~1,000,000 (peak 1) and a smaller peak with an apparent MW of ~100,000 (peak 2). Peak 1 was symmetrical and within the fractionation range of the column, but it spanned a wide size range, suggesting heterogeneity of the iron-bearing species. A similar assembly reaction was subsequently examined by analytical ultracentrifugation (fig. 5*B* and *C*). At sedimentation equilibrium, the plot of log A_{280} versus r^2 revealed two distinct slopes (fig. 5B) corresponding to two main species of ~1.1 MDa and ~96 kDa, close to the apparent MW of peak 1 and peak 2 in figure 5*A*. The two species accounted for 75% and 8%, respectively, of the A_{280} loaded in the ultracentrifugation cell, whereas the remaining 17% was distributed over a range of masses from 0.2–0.8 MDa (fig. 5*C*), consistent with the size range spanned by peak 1 (fig. 5*A*). Together with the data shown in fig. 2*D*, these results indicate that, under the experimental conditions used in these experiments, the mYfh1p monomer assembles into two predominant forms of ~1.1 MDa and ~100 kDa, corresponding to ~60 and ~6 mYfh1p subunits per macromolecule, respectively. Results of analytical ultracentrifugation of isolated Superdex 200 fractions corresponding to α_{60} (fig. 2*D; fractions 3–5*) confirmed the presence of a homogeneous species with an MW of ~1,100,000 (not shown).

The ~1.1-MDa Multimer Is a Regular Spherical Particle

For direct visualization of the 1.1-MDa species, Superdex 200 fractions corresponding to α_{60} were analyzed

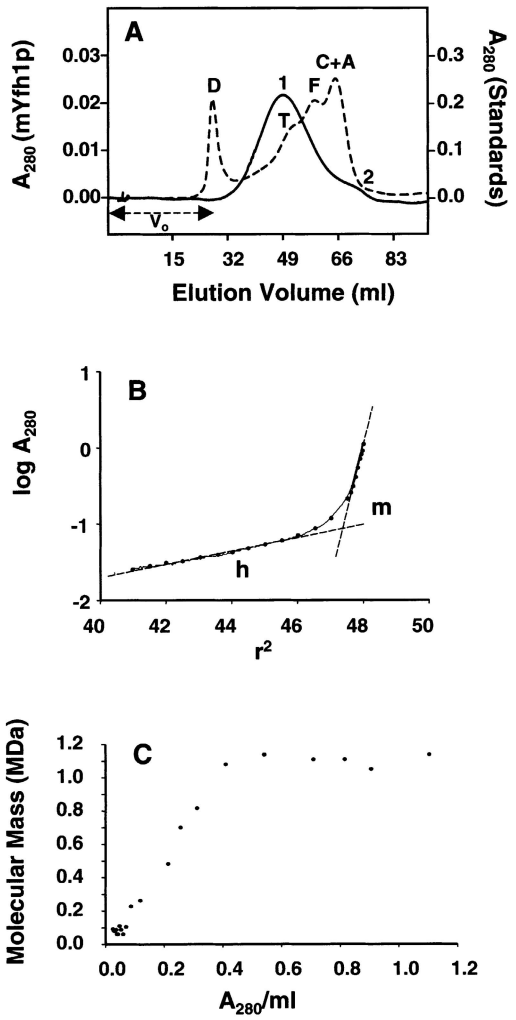

Figure 5 Gel filtration and sedimentation equilibrium analyses of Fe-mYfh1p. *A,* Experimental conditions were the same as those described in the legend for figure 2*C,* except that the sample was applied to a Superose 6 column. The elution profile of mYfh1p (*unbroken line*) is superimposed on that of MW standards (*broken line*). A = aldolase (158 kDa); C = catalase (232 kDa); F = ferritin (440 kDa); T = thyroglobulin (669 kDa); D = blue dextran 2,000 (2 MDa). *B,* Isolated mYfh1p was incubated with $Fe(NH_4)_2(SO_4)_2$, and the sample was subjected to sedimentation equilibrium analysis as described in the Material and Methods section. The plot of log A_{280} versus r^2 is shown. The presence of at least two different macromolecular species (multimer [m] and hexamer [h]) is deduced from two linear-fit lines. The slopes $(d\log A_{280})/[d(r^2)]$ correspond to m = 1.64 and h = 0.08. The equation $(2RT)/[(1-\bar{\nu}\rho)\varpi^2] \times [2.303(d\log A_{280})]/[d(r^2)]$ (Williams et al. 1958) was used to calculate the MW of the multimer and the hexamer. $\bar{\nu}$ = 0.73 cm^3/g, calculated from the amino acid composition of mYfh1p, was used for h, and $\bar{\nu}$ = 0.58 cm^3/g, including also 50 equivalents of FeO, was used for m. *C,* The molecular mass was also calculated at 22 different log A_{280}/r^2 increments (*blackened circles* in panel *B*) and was plotted versus the averaged A_{280}/ml. The m form, which accounts for ~75% of the total A_{280}, is denoted by the six blackened symbols at 1.1 MDa, and the h form, which accounts for ~8% of the A_{280}, is denoted by the cluster of blackened symbols at 0.1 MDa.

by EM and AFM. Electron micrographs of samples subjected to negative staining showed a homogeneous preparation of nearly circular particles (fig. 6*A*). By manually measuring the diameter of >150 particles, we obtained a range of values from 13–19 nm, with most (70%) of the particles ranging from 14.5–16 nm. Similar particles were observed in total assembly mixtures that had not been fractionated through the Superdex 200 column; no particles were detected in electron micrographs of isolated mYfh1p monomers (not shown). Individual particles appear to consist of an electron-dense ring surrounding an apparently empty cavity (fig. 6*B*). A concern regarding the use of this visualization method is that the negative staining procedure may result in artifacts. To exclude this possibility, a sample was placed onto a grid, air-dried, and imaged without further preparation. Electron micrographs of this sample showed circular electron-transparent particles that were similar to those viewed by negative staining (fig. 6*C*). The boundaries of individual particles were defined by small electron-dense granules (fig. 6*D*). The EM images shown in figure 6*A–D* suggest that the 1.1-MDa species identified by gel filtration and analytical ultracentrifugation is a spherical macromolecule. They also suggest that the iron associated with the 1.1-MDa species is in a dispersed form and that it concentrates at the periphery of the macromolecule. To obtain a tridimensional profile, the sample shown in figure 6*C* and *D* was also viewed by AFM. A large-scale AFM image is shown in figure 7*A,* and three-dimensional reconstructions are shown in figure 7*B* and *C.* Particles above a 5-nm threshold above the surface were counted, and the mean maximum height and full width at half height were determined. From analysis of 1,392 particles, we obtained a peak height of 12.8 ± 2.1 nm and a full width of 19.7 ± 13.4 nm. Vertical measurement from the AFM is the most accurate and sensitive, particularly for analysis of particles whose size is in the order of the radius of curvature of the AFM tip (~10 nm)—a condition that is known to cause spreading of the horizontal measurement (Radmacher et al. 1994). The mean peak height was in the order of the average diameter obtained by measuring particles visualized by negative staining and EM (fig. 6*A*). Thus, EM and AFM indicate that the ~1.1 MDa multimer is a regular spherical particle.

Detection of Fe-Yfh1p Complexes in Yeast Mitochondria

A detergent extract of wild-type yeast mitochondria was fractionated on the Superdex 200 column. Ten fractions (5 ml each) were collected, and the distri-

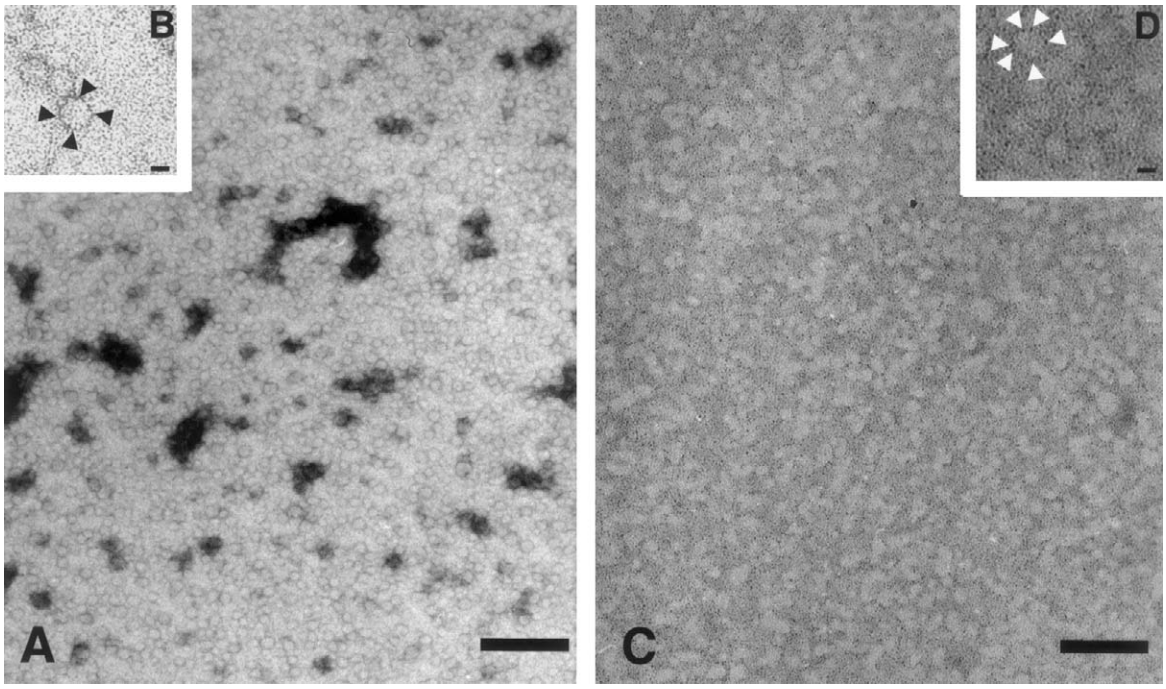

Figure 6 Electron microscopy of isolated Fe-mYfh1p multimers. Multimers were prepared and were isolated by gel filtration as described in the Material and Methods section. Aliquots were subjected to negative staining with 0.5% uranyl acetate (*A* and *B*), or they were simply dried on a grid and analyzed without further preparation (*C* and *D*). The initial magnification was × 50,000. In panels *A* and *C,* the bar = 100 nm, whereas in panels *B* and *D,* the bar = 10 nm.

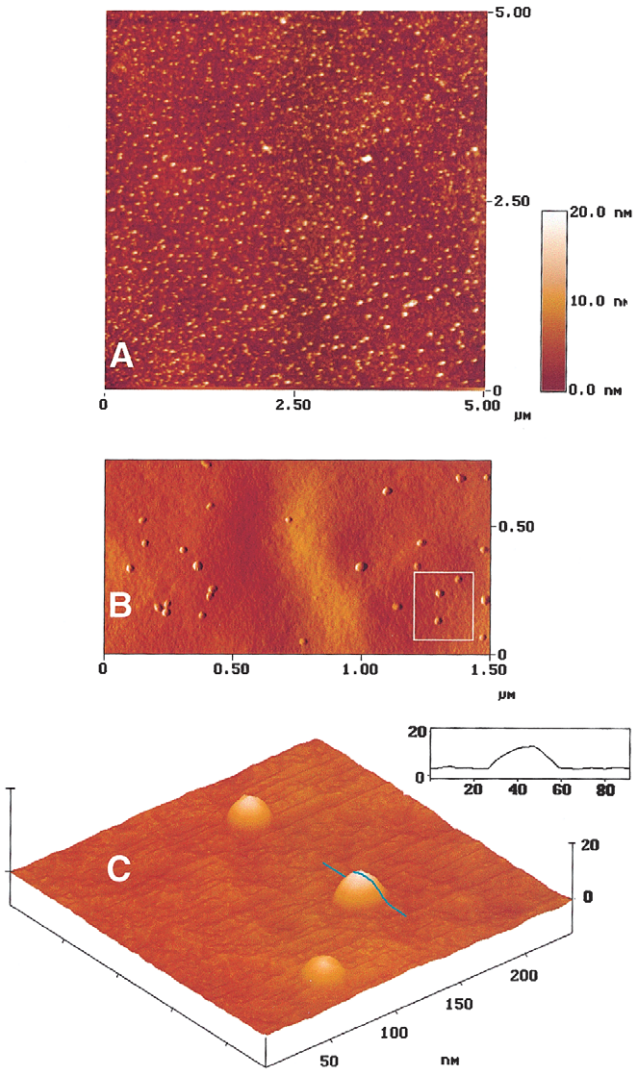

Figure 7 AFM of isolated Fe-mYfh1p multimers. The sample analyzed in figure 6*C* and *D* was viewed by AFM as described in the Material and Methods section. *A*, AFM image over an area of 5 × 5 μm. The height range is indicated by the inset. Three-dimensional AFM reconstruction from the top (*B*) and from a pitch angle of 33 degrees (*C*) are shown, and the procedure for measurement of width and height is illustrated by the profile of one particle (*C*, *inset*).

bution of endogenous mYfh1p was analyzed by western blotting (fig. 8*A*). Native mYfh1p was eluted in two peaks, with elution volumes corresponding to the monomer (fraction 8–9) and a higher species with MW >600,000 (fraction 1). As a control, the membrane was reprobed with an antibody against the β-subunit of MPP, a matrix-localized heterodimer consisting of one α-subunit (MW ~52,000), and one β-subunit (MW ~50,000) (Fenton and Kalousek 1996). A single protein peak was eluted in this case, with a peak maximum at ~100 kDa (fig. 8*A*, *fraction 5*), as was expected for the MPP holoenzyme. The distribution of endogenous mYfh1p was also analyzed in an Atm1-deficient strain (*atm*1Δ) that accumulates mitochondrial iron at levels ⩾10 times higher than the wild-type yeast (Kispal et al. 1997). Compared with the wild type, the monomer was decreased by ~50% (fig. 8*A*, *fractions 8–9*), and a larger proportion of mYfh1p was shifted to higher-MW species (fractions 1–7).

To analyze whether mYfh1p binds iron in vivo, mitochondria were prepared from *atm*1Δ cells grown in the presence of ^{55}Fe; as a result of low uptake of ^{55}Fe, this analysis was not performed in wild-type yeast. Mitochondrial extracts from *atm*1Δ cells were fractionated on the Superdex 200 column as described above. In three independent experiments, 25% of the added ^{55}Fe was accumulated in mitochondria (0.05 μmol), where it partitioned (1:4) between the soluble and insoluble membrane fractions. The soluble mitochondrial fraction was fractionated on the Superdex 200 column as described above, and 5-ml fractions were collected. The relative amounts of ^{55}Fe recovered in fractions 1–10 were very similar in three independent experiments, with most counts recovered in fractions 1, 5, and 6 (fig. 8*B*); this finding may reflect the presence of different iron-binding molecules in these three fractions. All fractions were initially incubated for 1 h with 100 μl protein A-Sepharose, to remove any ^{55}Fe that would nonspecifically bind to protein A or the Sepharose beads. This treatment was followed by immunoprecipitation with anti-Yfh1p antibodies and protein A-Sepharose. Significant levels of ^{55}Fe were recovered only in the immunocomplexes precipitated from fraction 1 (fig. 8*C*), which is the fraction that contains the high-MW form of mYfh1p (fig. 8*A*, *fraction 1*). In contrast, there was no significant recovery of ^{55}Fe in the immunocomplexes precipitated from the other fractions (fig. 8*C*). The ^{55}Fe associated with the immunoprecipitated high-MW form of mYfh1p represented 0.3% of the total (soluble plus insoluble) mitochondrial ^{55}Fe and 6% of the soluble mitochondrial ^{55}Fe. This value is significant, considering that *atm*1Δ mitochondria contain >10 times more iron than wild-type mitochondria (Kispal et al. 1997) and that the expression levels of mYfh1p were not increased in *atm*1Δ, compared with wild-type cells (fig. 8*A*). Estimates of the concentration of ^{55}Fe associated with the immunocomplexes from fraction 1 and the concentration of mYfh1p in this fraction yielded a molar Fe:mYfh1p ratio of ~16:1. The presence of both ^{55}Fe and nonradioactive iron in the immunoprecipitated complexes may explain why this ratio is lower than the ratio calculated for in vitro–assembled multimers (table 1). The lower ratio may also reflect the presence, in fraction 1, of species smaller than α_{60} (e.g., α_{24}, which has an Fe:mYfh1p ratio close to 16:1; see table 1), and experimental error may also

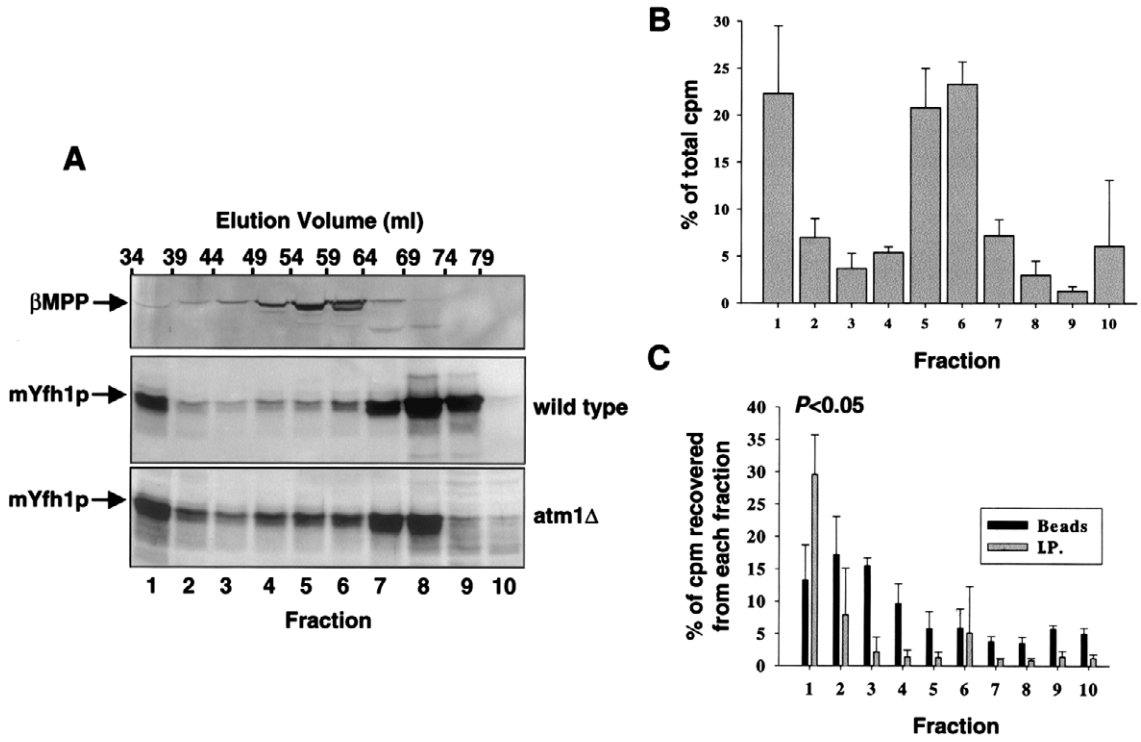

Figure 8 Detection of high-MW Fe-mYfh1p in vivo. *A,* Detergent extracts of isolated wild-type or *atm*1Δ mitochondria (~3 mg total protein in each case) were fractionated on a Superdex 200 column, and the eluted fractions were analyzed by western blotting. After detection of mYfh1p, the wild-type membrane was reprobed with a polyclonal antibody against β-MPP. *B* and *C,* Mitochondrial extracts were prepared from *atm*1Δ cells grown in the presence of $^{55}FeCl_3$ and were fractionated on a Superdex 200 column as described above. *B*, The cpm of each fraction were measured by scintillation counting and expressed as the percentage of the total cpm recovered in the 10 fractions analyzed ($0.8 - 1.6 \times 10^6$ cpm); the bars denote the means ± SD of three experiments. *C,* Fractions were pretreated with 100 μl protein A-Sepharose (beads), after which the supernatants (after removal of the beads) were incubated with anti-Yfh1p antibodies and immunocomplexes precipitated with another 100 μl protein A-Sepharose (I.P.). The cpm associated with the beads and I.P. pellets are expressed as the percentage of the total cpm in the corresponding fraction. The mean ± SD of three experiments is shown.

play a role. These results are consistent with the presence of high-MW Fe-mYfh1p in vivo.

Discussion

We have described the iron-dependent self-assembly of recombinant yeast frataxin (mYfh1p). Whereas isolated mYfh1p monomers contain no iron and show no significant tendency to self-associate, addition of ferrous iron to isolated mYfh1p results in the assembly of an ~1.1-MDa multimer that can sequester >3,000 atoms of iron in a soluble, stable, and available form. The possibility that this phenomenon arises from nonspecific aggregation has been excluded on the basis of the results of four different sets of experiments. We have shown that mYfh1p self-assembly is specifically induced by Fe^{2+}, whereas other divalent cations have no effect. Self-assembly of mYfh1p is a titratable process that depends on the molar Fe:mYfh1p ratio and not the absolute iron or protein concentration. This process yields regular multimers of reproducible iron:protein content, homogeneous molecular mass, and spherical shape. Iron can be mobilized from these multimers, and iron release results in multimer disassembly. The presence of a high-MW form of Fe-mYfh1p in isolated yeast mitochondria indicates that this process most likely reflects the physiological mechanism of yeast frataxin.

Probably the closest example to what we have observed is the iron-storage protein ferritin (Harrison and Arosio 1996). Ferritin monomers spontaneously assemble into a 24-subunit hollow multimer capable of storing up to 4,500 atoms of iron as a mineral core in its cavity (Harrison and Arosio 1996). The main apparent difference between ferritin and mYfh1p self-assembly is that the former takes place in the absence of iron (Harrison and Arosio 1996), whereas the latter is iron-dependent. In addition, the results of EM of Fe-mYfh1p multimers and findings from iron-release experiments suggest that the iron sequestered by mYfh1p is in a more dispersed and readily available form than is the iron bound to ferritin, which is generally difficult to mobilize in the absence of re-

ductants (Harrison and Arosio 1996). Nevertheless, the oxidation state of the iron stored in the mYfh1p multimers suggests a potential similarity to the iron-storage mechanism of ferritin. Electronic spectra and EPR analysis of mYfh1p multimers show the presence of oxo-bridged ferric iron, and, accordingly, iron-release experiments demonstrate that 60% of the sequestered iron is in the Fe^{3+} form. Oxo-bridged ferric iron species are found in ferritin and other binuclear iron proteins (Chasteen et al. 1985). Apo-ferritin multimers store iron by binding Fe^{2+} ions and by catalyzing their aerobic oxidation to oxo- and hydroxo-bridged ferric ions, which then polymerize inside the ferritin cavity to form a polyiron oxohydroxo mineral core (Chasteen et al. 1985; Harrison and Arosio 1996). We have found that self-assembly of isolated mYfh1p is induced by iron supplemented as $Fe(NH_4)_2(SO_4)_2$ or $FeCl_2$, whereas addition of $FeCl_3$ causes protein precipitation (unpublished data). Therefore, we speculate that self-assembly is initiated by Fe^{2+} binding to mYfh1p and by its oxidation to Fe^{3+}, leading to formation of polyiron oxohydroxo clusters faster than formation of insoluble ferric oxyhydroxides. Studies addressing ferroxidase activity and ability to assemble under anaerobic conditions are under way to test this hypothesis. Because we did not detect any iron bound to mYfh1p monomers, we conclude that two or more subunits must be involved in the initial Fe^{2+} binding. The smallest iron-containing species that we detected is the mYfh1p trimer, which is formed at Fe:mYfh1p ratios of 1:1. The results of titration experiments suggest a stepwise mechanism of mYfh1p self-assembly, with the trimer representing the initial assembly unit. Because the iron content of the multimer (~3,000 atoms) is 10-fold higher than the total iron content of 20 trimers (~300 atoms), the assembly process must also involve some structural changes that expand the initial iron-loading capacity. Of interest, the results of our iron-release experiments show that the mYfh1p multimers contain not only Fe^{3+} ions but, also, a smaller population of Fe^{2+} atoms. Reduced iron could be bound in a hydrophobic environment within the protein where oxygen is not readily accessible. A similar mechanism has been proposed to explain the ability of the enzyme ferrochelatase to keep iron in a reduced form, as is required for its attachment to protoporphyrin IX to yield heme (Romslo 1980). Thus, mYfh1p multimers could stabilize ferrous iron via its oxidation to oxo-bridged ferric species and, at the same time, could maintain a smaller supply of Fe^{2+} atoms.

The properties described above would be ideal for a role of Yfh1p in mitochondrial iron management. Most mitochondrial iron is normally bound in cytochromes and iron-sulfur proteins in the inner and outer membranes and to the iron-sulfur protein aconitase in the matrix. A smaller fraction of nonheme non-FeS iron is believed to represent the main source of bioavailable iron inside mitochondria (Tangeras 1985). In rat liver mitochondria, this fraction is distributed between the inner membrane and the matrix, and it corresponds to 40% of the total mitochondrial iron (Tangeras 1985). In our immunoprecipitation experiments, 6% of the soluble mitochondrial ^{55}Fe accumulated in *atm*1Δ mitochondria was associated with high-MW mYfh1p. Because *atm*1Δ mitochondria contain normal levels of mYfh1p but accumulate 10 times more iron than do wild-type mitochondria, the fraction of iron normally bound to mYfh1p may be higher than we have determined. Similarly, the molar Fe:mYfh1p ratio in native Fe-mYfh1p complexes is probably higher than the estimated ratio of 16:1, because this value takes into account only the radioactive iron atoms bound in the complexes. Even though a precise determination of the Fe:mYfh1p stoichiometry in vivo must await purification of sufficient amounts of native complexes, the data support a model in which mYfh1p binds uncomplexed iron and stores it in a bioavailable form.

This model may seem difficult to reconcile with observations that deletion of Yfh1p (*yfh*1Δ) results in mitochondrial iron accumulation (Babcock et al. 1997; Foury and Cazzalini 1997). The primary effect of Yfh1p deletion, however, is a loss of mitochondrial iron export; mitochondrial iron accumulation is a secondary effect resulting from cytoplasmic iron starvation and induction of the plasma membrane high-affinity iron transporter FET3 (Foury 1999; Radisky et al. 1999; Chen and Kaplan 2000). Thus, the ability of recombinant mYfh1p to bind iron and to maintain it in a soluble and available form in vitro is consistent with the role played by native Yfh1p in iron export and could also account for a proposed role in iron-sulfur cluster biosynthesis (Foury 1999). The oxidative damage associated with frataxin deficiency in FRDA (Rotig et al. 1997; Bradley et al. 2000) implies that, in storing uncomplexed iron, Yfh1p should also prevent iron toxicity. We have found that, by complexing Fe^{2+}, recombinant mYfh1p inhibits hydroxyl radical formation from Fenton chemistry (manuscript in preparation). Thus, the iron-dependent self-assembly of mYfh1p in vitro may reflect physiological roles in mitochondrial iron bioavailability and protection from iron-induced oxidative damage.

Acknowledgments

We thank F. Kalousek, for discussions and anti-MPP antibodies; D. Koeller, for the *atm*1Δ mutant; and A. Borovik, for critical reading of the manuscript. ICP was performed at the Mayo Metal Laboratory; amino acid analysis, at the Mayo Protein Core; and radiosequencing, at the Biotechnology Re-

source Laboratory at Yale University. This work was supported by grant AG15709 from the National Institute on Aging.

Electronic-Database Information

Accession numbers and URLs for data in this article are as follows:

GenBank, http://www.ncbi.nlm.nih.gov/Genbank/index.html (for *YFH1* [accession number Z74168])
Online Mendelian Inheritance in Man (OMIM), http://www.ncbi.nlm.nih.gov/Omim/ (for FRDA [MIM 229300])

References

Babcock M, de Silva D, Oaks R, Davis-Kaplan S, Jiralerspong S, Montermini L, Pandolfo M, Kaplan J (1997) Regulation of mitochondrial iron accumulation by Yfh1p, a putative homologue of frataxin. Science 276:1709–1712

Bradley JL, Blake JC, Chamberlain S, Thomas PK, Cooper JM, Schapira AH (2000) Clinical, biochemical and molecular genetic correlations in Friedreich's ataxia. Hum Mol Genet 9:275–282

Branda SS, Cavadini P, Adamec J, Kalousek F, Taroni F, Isaya G (1999) Yeast and human frataxin are processed to mature form in two sequential steps by the mitochondrial processing peptidase. J Biol Chem 274:22763–22769

Campuzano V, Montermini L, Lutz Y, Cova L, Hindelang C, Jiralerspong S, Trottier Y, Kish SJ, Faucheux B, Trouillas P, Authier FJ, Durr A, Mandel JL, Vescovi A, Pandolfo M, Koenig M (1997) Frataxin is reduced in Friedreich ataxia patients and is associated with mitochondrial membranes. Hum Mol Genet 6:1771–1780

Campuzano V, Montermini L, Molto MD, Pianese L, Cossee M, Cavalcanti F, Monros E, et al (1996) Friedreich's ataxia: autosomal recessive disease caused by an intronic GAA triplet repeat expansion. Science 271:1423–1427

Chasteen ND, Antanaitis BC, Aisen P (1985) Iron deposition in apoferritin: evidence for the formation of a mixed valence binuclear iron complex. J Biol Chem 260:2926–2929

Chen OS, Kaplan J (2000) CCC1 suppresses mitochondrial damage in the yeast model of Friedreich's ataxia by limiting mitochondrial iron accumulation. J Biol Chem 275:7626–7632

de Silva DM, Askwith CC, Kaplan J (1996) Molecular mechanisms of iron uptake in eukaryotes. Physiol Rev 76:31–47

Fenton WA, Kalousek F (1996) Proteolytic processing of mitochondrial precursor proteins. Adv Mol Cell Biol 17:163–191

Foury F (1999) Low iron concentration and aconitase deficiency in a yeast frataxin homologue deficient strain. FEBS Lett 456:281–284

Foury F, Cazzalini O (1997) Deletion of the yeast homologue of the human gene associated with Friedreich's ataxia elicits iron accumulation in mitochondria. FEBS Lett 411:373–377

Gavel Y, von Heijne G (1990) Cleavage-site motifs in mitochondrial targeting peptides. Protein Eng 4:33–37

Hansma HG, Hoh JH (1994) Biomolecular imaging with the atomic force microscope. Annu Rev Biophys Biomol Struct 23:115–139

Harrison PM, Arosio P (1996) The ferritins: molecular properties, iron storage function and cellular regulation. Biochim Biophys Acta 1275:161–203

Kispal G, Csere P, Guiard B, Lill R (1997) The ABC transporter Atm1p is required for mitochondrial iron homeostasis. FEBS Lett 418:346–350

Knight SA, Sepuri NB, Pain D, Dancis A (1998) Mt-Hsp70 homolog, Ssc2p, required for maturation of yeast frataxin and mitochondrial iron homeostasis. J Biol Chem 273:18389–18393

Koutnikova H, Campuzano V, Foury F, Dolle P, Cazzalini O, Koenig M (1997) Studies of human, mouse and yeast homologues indicate a mitochondrial function for frataxin. Nat Genet 16:345–351

Koutnikova H, Campuzano V, Koenig M (1998) Maturation of wild-type and mutated frataxin by the mitochondrial processing peptidase. Hum Mol Genet 7:1485–1489

Kozak M (1987) At least six nucleotides preceding the AUG initiator codon enhance translation in mammalian cells. J Mol Biol 196:947–950

Lamarche JB, Cote M, Lemieux B (1980) The cardiomyopathy of Friedreich's ataxia morphological observations in 3 cases. Can J Neurol Sci 7:389–396

Matsudaira P (1987) Sequence from picomole quantities of proteins electroblotted onto polyvinylidene difluoride membranes. J Biol Chem 262:10035–10038

Nixon DE, Moyer TP, Johnson P, McCall JT, Ness AB, Fjerstad WH, Wehde MB (1986) Routine measurement of calcium, magnesium, copper, zinc, and iron in urine and serum by inductively coupled plasma emission spectroscopy. Clin Chem 32:1660–1665

Radisky DC, Babcock MC, Kaplan J (1999) The yeast frataxin homologue mediates mitochondrial iron efflux: evidence for a mitochondrial iron cycle. J Biol Chem 274:4497–4499

Radmacher M, Fritz M, Hansma HG, Hansma PK (1994) Direct observation of enzyme activity with the atomic force microscope. Science 265:1577–1579

Richards TD, Pitts KR, Watt GD (1996) A kinetic study of iron release from Azotobacter vinelandii bacterial ferritin. J Inorg Biochem 61:1–13

Romslo I (1980) Intracellular transport of iron. In: Jacobs A, Worwood M (eds) Iron in biochemistry and medicine. Academic Press, London, pp 325–362

Rotig A, de Lonlay P, Chretien D, Foury F, Koenig M, Sidi D, Munnich A, Rustin P (1997) Aconitase and mitochondrial iron-sulphur protein deficiency in Friedreich ataxia. Nat Genet 17:215–217

Sanders-Loehr J (1989) Binuclear iron proteins. In: Loehr T (ed) Iron carriers and iron proteins from physical inorganic chemistry, vol 5. VCH Publishers, New York, pp 373–466

Tangeras A (1985) Mitochondrial iron not bound in heme and iron-sulfur centers and its availability for heme synthesis in vitro. Biochim Biophys Acta 843:199–207

Veenstra TD, Benson LM, Craig TA, Tomlinson AJ, Kumar R, Naylor S (1998) Metal mediated sterol receptor-DNA complex association and dissociation determined by electrospray ionization mass spectrometry. Nat Biotechnol 16:262–266

Wallace DC, Melov S (1998) Radicals r'aging. Nat Genet 19:105–106

Williams JW, Van Holde KE, Baldwin RL, Fujita H (1958) The theory of sedimentation analysis. Chemical Review 58: 715–806

Wong A, Yang J, Cavadini P, Gellera C, Lonnerdal B, Taroni F, Cortopassi G (1999) The Friedreich's ataxia mutation confers cellular sensitivity to oxidant stress which is rescued by chelators of iron and calcium and inhibitors of apoptosis. Hum Mol Genet 8:425–430